Some New Aspects of Product Distribution Functions for Three-Atom Unimolecular Reactions Performed in Beam Experiments

L. Bonnet* and J. C. Rayez

Laboratoire de Physicochimie Théorique, URA 503, Université Bordeaux 1 and CNRS, 33405 Talence Cedex, France

Received: April 9, 1997; In Final Form: September 10, 1997[⊗]

Energy distribution functions for the products in two classes of three-atom unimolecular reactions performed in beam experiments are derived which are much more realistic than the prior distribution functions (PDF) of Levine and Bernstein without being more complicated. In a first step, we deal with light-atom emission processes governed by short-range forces. Contrary to what is generally believed, we emphasize the applicability of statistical theory of energy distributions to such reactions in which the change in energy partitioning from critical configuration to products is weak if not negligible. In a second step, we treat within the framework of phase space theory (PST) the more usual case of processes governed by long-range forces for which, however, there exists no realistic distribution functions. Comparison with experimental results or with results of simulations and/or results obtained using PDF, PST, or the statistical adiabatic channel model (SACM) is done for the following processes: (i) $C_2H \rightarrow C_2 + H$ (model alkyl dissociation reaction), (ii) $O_2H \rightarrow O_2 + H$, (iii) $NO_2 \rightarrow NO + O$, and (iv) $Al_3 \rightarrow Al_2 + Al$. For reaction i which proceeds through a barrier and for reaction ii which is barrierless but involves strong angular anisotropies in the exit-channel part of the potential energy surface, the distributions derived by our method are much more realistic than those obtained using PST or SACM.

I. Introduction

Energy distributions among the products of unimolecular reactions performed in beam experiments are part of the reduced set of experimentally available microcanonical informations on chemical reactions.[1] The research of the main factors governing these distributions is a necessary step toward a better understanding of gas-phase chemical reactivity.[1−4]

For processes governed by long-range forces and involving a long-lived energized molecule before dissociation, the statistical theory of molecular collisions[1,5−13] is perhaps the best compromise for the qualitative/quantitative study of product energy partitioning.[14] Indeed, this theory is interpretative in nature since it is based on several assumptions, the main ones being energy randomization and the concept of transition state (TS). Moreover, the simplicity of the numerical calculations involved permits the study of how energy distributions vary with parameters such as translational energy of the reagents, exoergicity (for bimolecular reactions), atomic masses, dispersion constants, etc.[15] Also, some key steps in the development of the theory lead straightforwardly to the role of angular momentum constraints. Last but not least, further assumptions may allow the simplification of the developments, the ultimate stage being the derivation of simple formulas[15] where the preponderant factors of interest appear explicitly.

For processes proceeding through a tight TS corresponding, for instance, to a barrier, the dynamics associated with system motion from critical configuration to products—referred to as exit-channel coupling effects[16]—modify in most cases the energy partitioning as the system dissociates. Though a statistical treatment can be used to predict energy distributions at the TS, there is no simple analytical way to deduce their distortions upon passing from TS to products. Hence, there is no general statistical theory of energy distributions applicable to any process governed by short-range forces as noted in the recent exhaustive review by Baer and Hase.[17]

We have shown recently, however, that the rule regarding the modification of energy partitioning admits some exceptions, namely reactions of the kind $ABC \rightarrow AB + C$ where C is a light atom (typically a hydrogen atom) for which exit-channel coupling effects are very often negligible whether there is a barrier or not.[18] The reasons why this is so are related to the short time of residence of the system on the product side of the critical region (at the usual energies of ≈ 1 eV) and to the weak efficiency of the impulsive mechanism of repulsion between B and C (see section II.B).[19] Energy distributions are thus expected to be roughly the same at the TS and in the products, which does not mean that conventional methods such as phase space theory (PST) which deal with loose TS can be applied. This is why we devised a method for calculating the recoil energy distribution at the TS[18] (and thus in the final products) which, to our knowledge, did not previously exist.

The main goal of the present article is to support our previous analysis in the light of the two following processes

$$C_2H \rightarrow C_2 + H \qquad \text{(I.1)}$$

(model alkyl dissociation reaction) and

$$O_2H \rightarrow O_2 + H \qquad \text{(I.2)}$$

extensively studied by Wolf and Hase[20a,b] and Hamilton and Brumer[20c] (I.1) and Schinke et al.[21] (I.2). Such a work requires first the extension of our method to three-atom unimolecular processes performed in beam experiments for which the total angular momentum is roughly negligible (reactions I.1 and I.2 have been studied using this assumption).[22] Due to the simplicity of the problem, we are able to derive energy distribution functions, i.e., analytical expressions where the preponderant factors governing the dynamics appear explicitly

[⊗] Abstract published in *Advance ACS Abstracts,* November 15, 1997.

S1089-5639(97)01200-0 CCC: $14.00

(see Table 1 in section II.B). In this regard, they are much more realistic than the prior distribution functions (PDF) of Levine and Bernstein[23] without being much more complicated. We also deal within the framework of PST with the more usual case of reactions governed by long-range forces for which, however, a similar treatment does not exist (see Table 2 in section II.C). The first set of distributions is applied to reactions I.1 and I.2 (section III.A) whereas the second set is applied to the following processes (section III.B):

$$NO_2 \rightarrow NO + O \tag{I.3}$$

and

$$Al_3 \rightarrow Al_2 + Al \tag{I.4}$$

studied by Reid, Reisler, and co-workers[24] (I.3) and Peslherbe and Hase[25] (I.4). Comparison is done between our method and (a) dynamical calculations or experimental results and (b) standard statistical theories such as the PDF method, PST, or statistical adiabatic channel model (SACM). A conclusion follows (section IV). The paper may be understood without the need to read the final appendices where the mathematical developments are presented.

II. Energy Distribution Functions

A. Bases. The process of interest is of the type ABC → ABC* → AB + C. In practice, jet-cooled ABC molecules are optically excited to a pure vibrational level at an energy E' in excess of the dissociation energy D_0, followed by the unimolecular reaction ABC* → AB + C.[24] The energy excess with respect to the zero-point level of AB is $E = E' - D_0$. E_0 being the zero-point energy, the energy disposal with respect to the bottom of the product channel is thus $E_P = E + E_0$. In such experiments, the average magnitude of the total angular momentum **J** is most of the time so low (about 5 h units for NO_2[26]) that we keep it at zero.[22] This assumption considerably simplifies the developments. The coordinate system used in this paper is given in the first section of Appendix A.

In the interval between the optical excitation and the final dissociation, ABC* is supposed to wander about in the region of the phase space associated with the strong coupling region (SCR). Consequently, the products are equally likely to be on any trajectory emerging from the SCR, that is, crossing the TS or dividing surface delimiting the SCR in the direction of the products. The density of probability that given observables Q_1, ..., Q_N have the values q_1, ..., q_N at the transition state is thus given by

$$P(q_1, ..., q_N) = \frac{F(q_1, ..., q_N, E)}{F(E)} \tag{II.1}$$

where $F(q_1, ..., q_N, E)$ is the flux of trajectories crossing the TS with $Q_1 = q_1$, ..., $Q_N = q_N$ and E, and $F(E)$ is the total flux of trajectories crossing the TS with E. In this work, the Q_i's are limited to scalar observables, that is, the vibrational energy E_V of AB, j—or equivalently the rotational energy E_R of AB—and the recoil energy E_T of C with respect to AB. The general procedure adopted in this paper for the calculation of both the numerator and the denominator of eq II.1 is presented in Appendix A.

B. Light-Atom Emission Processes Governed by Short-Range Forces. For reactions governed by short-range forces, involving for instance a barrier between reactants and products, there are in the general case changes in energy partitioning as the system proceeds from TS to products. These changes are often referred to as exit-channel coupling effects.[16] Applying the microcanonical postulate of statistical mechanics to the strong coupling region (SCR) allows for calculating the distribution of the energy at the TS but there is no simple way to calculate analytically the transformations this distribution undergoes from the critical configuration onto the products. However, we have shown recently[18] that when (i) the system has a linear geometry at the saddle point and (ii) C is very light with respect to A and B (typically a hydrogen atom), the energy partitioning does not evolve significantly on the way from the critical configuration to the products. Feature i causes the modification of the rotational angular momentum of AB to be inefficient when B and C repel each other (no impulsive mechanism) and feature ii makes the relative velocity of C with respect to AB sufficiently large for the time of residence of the system on the product side of the barrier to be very short (for the usual values of the kinetic energy, say ≈ 1 eV). In that region, the torque the rotating diatomic AB creates on the departing atom C thus has no time for the rotational angular momentum of AB and orbital angular momentum of C with respect to AB to exchange motion. Since (a) j does not vary between the TS and the products and (b) vibrational degrees of freedom are usually weakly coupled to the remainder of the Hamiltonian (see Appendix A), the translational energy is also expected to reach its final value at the critical configuration. In that case, product energy distributions are identical with energy distributions at the TS.

The way the energy is partitioned at the TS is central for the determination of the distributions. As shown in ref 18 and in section 2 of Appendix A, *it is very important to include the potential energy of interaction between C and the rigid rotor AB in the translational energy, in addition to the purely kinetic terms* (see eqs A.1 and A.5). When the system is at the TS, a large part of the translational energy is in the potential energy. During the repulsion between C and AB, the potential energy decreases and the kinetic energy increases such that their sum E_T does not vary (we are still assuming that C is very light). It is then meaningless to compare the distribution of the kinetic energy at the TS with that in the products, the later being obviously much more excited than the former. Using the quasi-classical trajectory (QCT) method, Wolf and Hase were the first[20b] to observe that the sum of the barrier height V_0 and the kinetic energy at the TS led to a value in good agreement with the product translational energy. However, replacing V_0 by the potential energy of interaction mentioned above (see eq A.1) leads to an even better agreement.[18]

The distribution functions of interest are derived in Appendix B and are collected in Table 1. The only assumption used is a harmonic angular dependence of the potential energy at the TS.

As shown further below, feature i (linear geometry at the saddle point) is not a necessary condition for the validity of the formulation (reaction I.2, which does not involve a linear TS, is well-described by our method). Feature i guarantees, however, an even better agreement between the model and the dynamical calculations.

C. Reactions Governed by Long-Range Forces. PST is the simplest microcanonical statistical theory of chemical reactions governed by long-range forces.[5,6,9,10,13] One of the main assumptions of PST we shall adopt here is that the potential energy of interaction between AB and C is of the kind $V(R) = -C_n/R^n$. Though the angular dependence of the potential energy is not taken into account, PST has often been shown to lead to accurate energy distributions.

Consider the reverse reaction of recombination AB + C → ABC. The maximum value of the orbital angular momentum

TABLE 1: Energy Distributions among the Products of Three-Atom Unimolecular Reactions ABC → AB + C Involving a Barrier along the Reaction Path Separating the Well and the Products[a]

I	$\left(\frac{1}{mr_e^{\ddagger 2}}+\frac{1}{\mu R^{\ddagger 2}}\right)^{-1}$
$P(j,E_V)$	$\frac{2^{5/2}}{\pi(E-V_0)^2 I^{1/2}}\left(E_P-V_0-E_V-\frac{j^2}{2I}\right)^{1/2}$
$P(j)$	$\frac{2^{7/2}}{3\pi(E-V_0)^2 I^{1/2}}\left(E-V_0-\frac{j^2}{2I}\right)^{3/2}$
$P(E_R)$	$\frac{8((1-\rho)(E-V_0)-E_R)^{3/2}}{3\pi(E-V_0)^2(1-\rho)^2 E_R^{1/2}}$ with $\rho=\frac{mr_e^2}{mr_e^2+\mu R^{\ddagger 2}}$
$P(E_V)$	$\frac{2}{(E-V_0)^2}(E_P-V_0-E_V)$
$P(E_T)$	$\frac{\pi}{2}(1-\rho)^{1/2}(E_T-V_0)$ if $E_T \le (1-\rho)V_0+\rho E$
	$\left(\frac{\rho(E-E_T)}{1-\rho}(E_T-(1-\rho)V_0-\rho E)\right)^{1/2}+$
	$\left((1-\rho)^{1/2}(E_T-V_0)\left(\frac{\pi}{2}-\right.\right.$
	$\left.\left.\arcsin\left[\left(\frac{E_T-(1-\rho)V_0-\rho E}{(1-\rho)(E_T-V_0)}\right)^{1/2}\right]\right)\right)$
	if $E_T > (1-\rho)V_0+\rho E$

[a] C is assumed to be very light with respect to A and B (typically a hydrogen atom). E_P is the product energy disposal, that is, the sum of E_V, E_T, and E_R. E is the excess energy equal to $E_P - E_0$ where E_0 is the zero-point energy of AB. m and μ are, respectively, the reduced masses of AB and C with respect to AB. r_e is the equilibrium distance of AB. V_0 is the barrier height, i.e., the energy difference between the saddle point and the bottom of the products valley.

L consistent with the recombination at E_T is (for more details, see ref 13 and references therein)

$$L_M(E_T) = b_M(E_T)\,(2\mu E_T)^{1/2} \qquad \text{(II.2)}$$

where $b_M(E_T)$, the maximum value of the impact parameter consistent with the capture at E_T, is given by

$$b_M(E_T) = \left[\frac{n-2}{n}\right]^{(2-n)/2n}\left[\frac{nC_n}{2E_T}\right]^{1/n} \qquad \text{(II.3)}$$

Replacing $b_M(E_T)$ in eq II.2, by its average value $b_{av}(E)$

$$b_{av}(E) = \int_0^E \mathrm{d}E_T \frac{b_M(E_T)}{E} = \frac{n^{3/2}(n-2)^{(2-n)/2n}}{n-1}\left(\frac{C_n}{2E}\right)^{1/n} \qquad \text{(II.4)}$$

does not modify qualitatively the shape of $L_M(E_T)$ which results in

$$L_M(E_T) \approx b_{av}(E)\,(2\mu E_T)^{1/2} \qquad \text{(II.2')}$$

The reason is that the approximate $L_M(E_T)$ depends on $E_T^{1/2}$ whereas the exact one depends on $E_T^{(1/2-1/n)}$ (see eqs II.2 and II.3). Moreover, the larger n is, the lower the quantitative difference.

Equation II.2′ suggests that the mechanism of capture is correctly described by the following assumption: two fragments colliding with an impact parameter b larger than b_{av} (b_{av} stands for $b_{av}(E)$ in the following) do not feel any mutual interaction all along their motion. On the other hand, a value of b lower than or equal to b_{av} makes the probability of capture equal to one. The TS is thus defined by $R^{\ddagger} \approx b_{av}$ and $V(R^{\ddagger}) \approx 0$.

TABLE 2: Energy Distributions in the Products of Three-Atom Unimolecular Reactions ABC → AB + C Governed by Isotropic Long-Range Forces[a]

b_{av}	$\frac{n^{3/2}(n-2)^{(2-n)/2n}}{n-1}\left(\frac{C_n}{2E}\right)^{1/n}$
I	$\left(\frac{1}{mr_e^2}+\frac{1}{\mu b_{av}^2}\right)^{-1}$
$P(j,E_V)$	$\frac{3}{(2E)^{3/2} I^{1/2}}$ with $E_0 \le E_V \le E_P - \frac{j^2}{2I}$
$P(j)$	$\left(\frac{3}{(2E)^{3/2} I^{1/2}}\right)\left(E-\frac{j^2}{2I}\right)$
$P(E_R)$	$\frac{3((1-\rho)E-E_R)}{4((1-\rho)E)^{3/2} E_R^{1/2}}$ with $\rho=\frac{mr_e^2}{mr_e^2+\mu b_{av}^2}$
$P(E_V)$	$\left(\frac{3}{2E^{3/2}}\right)(E_P-E_V)^{1/2}$
$P(E_T)$	$\left(\frac{3}{(2E_P)^{3/2} I^{1/2}}\right)\min[b_M(2\mu E_T)^{1/2};\, r_e(2m(E-E_T))^{1/2}]$

[a] That is, those involving a potential energy between AB and C of the kind $V(R) = -C_n/R^n$. M, μ, r_e, E_P and E are defined in the footnote to Table 1.

TABLE 3. Parameters Used in the Calculations of Energy Distribution Functions[a]

reaction	m	μ	r_e	$R^{\ddagger}$	C_6	V_0
I.1	6	≈1	1.33	2.7		3.5
I.2	8	≈1	1.33	2.2		0
I.3	7.47	10.43	1.21		496	
I.4	13.5	18	2.6		38153	

[a] m and μ are in atomic mass units, r_e and $R^{\ddagger}$ in angstroms, C_6 in kcal mol^{-1} Å^{-6}, and V_0 in kcal mol^{-1}.

According to the principle of microreversibility, this TS is also the one for the dissociation process.

The assumption above allows for deriving energy distribution functions as shown in Appendix C. These functions are collected in Table 2.

III. Application to Some Processes

A. Processes Governed by Short-Range Forces. Reaction I.1 ($C_2H \rightarrow C{=}C + H$) is a prototype of radical alkyl dissociation processes such as $C_2H_5 \rightarrow C_2H_4 + H$. It has been studied theoretically by Wolf and Hase on various model potential energy surfaces, using the QCT method.[20a,b] The results considered here are the recoil and vibrational energy distributions $P(E_T)$ and $P(E_V)$ obtained by Hamilton and Brumer[20c] using the surface II.A which involves a barrier of 3.5 kcal/mol along the reaction path. The geometry of the system at the saddle point is linear. The total energy E_p has been kept at 10 kcal/mol. Since we are dealing with classical trajectories, there is no zero-point level and the energy excess E reduces to E_p. The other parameters required for the calculation of $P(E_V)$ and $P(E_T)$ (see Table 1) are given in the first row of Table 3.

Comparison between (i) our energy distribution functions, (ii) those found using PST, and (iii) QCT calculations is given in Figure 1. Contrary to PST, our formulation leads to an excellent agreement between statistical energy distributions and the QCT results. Hamilton and Brumer[20c] claim that exit-channel coupling effects are responsible for the discrepancies observed between PST and QCT distributions. From our point of view, this interpretation is questionable since in the very present case exit-channel coupling effects are negligible. As a matter of fact, neither the orbital angular momentum of H with

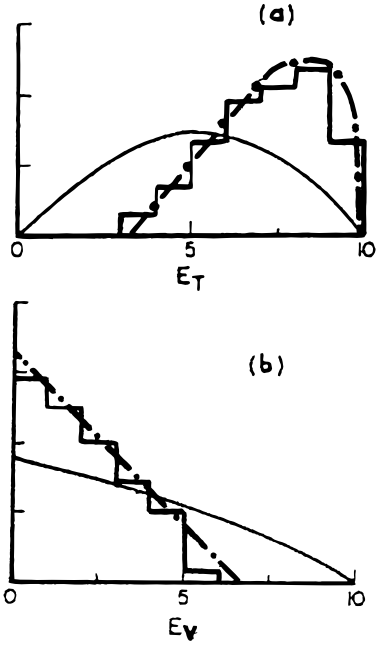

Figure 1. Translational (a) and vibrational (b) energy distributions in the products of the model reaction $C_2H \rightarrow C_2 + H$; QCT (histograms); PST (solid lines); our method (dashed−dotted lines).

respect to C_2 nor the rotational angular momentum of C_2 vary significantly from the TS to the separated products.[20b] Moreover, *the distributions we calculate at the TS from our method are the same as those found in the products by the QCT method,* which tends to prove that both recoil and vibration energies are conserved during the CH bond cleavage. Hamilton and Brumer proposed a statistical dynamical approach called "exit channel corrected PST" (ECCPST).[20c] This method consists of running trajectories from the product phase space, the initial conditions being sampled microcanonically. The trajectories which do not reach the critical configuration are discarded and the statistical distributions in the products are built from the initial conditions of the remaining trajectories. As a matter of fact, ECCPST leads to the same distributions as those found from our method. In other words, the distributions do not evolve from the products to the TS, and by microreversibility, we arrive at the same conclusion as above, namely energy transfers are inefficient upon passing from TS to products. The same conclusion can be deduced for the rotational energy distribution.

Reaction I.2 ($O_2H \rightarrow O_2 + H$) has been studied theoretically by the Schinke group.[21] This is certainly the most complete theoretical study of a three-atom unimolecular reaction performed so far. They largely focus their analysis on the distribution of the product rotational angular momentum. Concerning the shape of the DMBE IV potential energy surface of Pastrana et al.[27] in the transition state area, it turns out that there is no barrier along the reaction paths defined by two values of the angle ϕ between GH and OO (G is the center of mass of O_2), namely 55° and 125°, as can be seen in Figure 18 of ref 21 where γ has the same meaning as ϕ. There is however, a hill between these two paths, the top of which corresponds to $\phi = 90°$. In other words, there is a barrier along the path defined by $\phi = 90°$. Therefore, this reaction is intermediate between those governed by long-range attractive forces and those governed by short-range repulsive forces, and the expressions given in Table 1 cannot be applied directly. Instead, we shall consider the following reasoning.

As explained in Appendix A, E_V is supposed to be weakly coupled to E_R and E_T from the TS onto the products. The

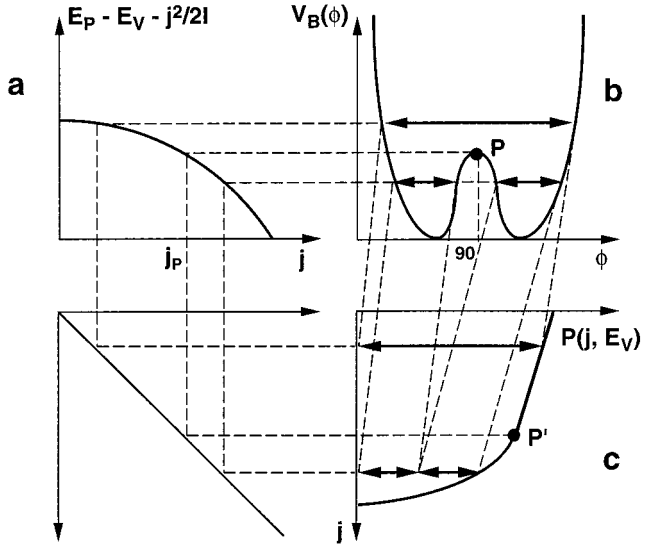

Figure 2. Scheme depicting the calculation of the rotational energy distribution $P(j,E_V)$ as explained in the text.

potential energy $V(R,r,\phi)$ can therefore be written as

$$V(R,r,\phi) \approx v(r) + V(R,r_e,\phi) \quad \text{for} \quad R \geq R^{\ddagger} \qquad \text{(III.A.1)}$$

where $v(r)$ is the free AB diatomic potential energy, $V(R,r_e,\phi)$ is the interaction potential energy between the rigid rotor AB (kept at its equilibrium distance r_e) and C, and $R^{\ddagger}$ gives the position of the TS. The potential energy $V(R,r_e,\phi)$ in the region of the TS is roughly the sum of (a) an isotropic attrative term $V_A(R) = V(R,r_e, 55° \text{ or } 125°)$ like those involved in processes governed by long-range forces, of which the dependence with respect to R is that of $V(R,r_e,\phi)$ along the reaction paths and (b) an angular dependent term $V_B(\phi) = V(R^{\ddagger},r_e,\phi)$ accounting for the bending motion. To the attractive term $V_A(R)$, we apply the assumption introduced in section II.C, i.e., the system behaves as if $V_A(R) \approx 0$ at the TS, found to be located at $R^{\ddagger} \approx$ 2.2 Å by Dobbyn et al.[21] Thus, the potential energy at the TS reduces to $V_B(\phi)$. Its dependence in terms of ϕ is the same as in Figure 18 of ref 21, the only difference being that $V_B(55°) = V_B(125°) = 0$ eV instead of ≈ -0.13 eV.

From eqs A.17 and II.1, the probability distribution $P(j,E_v)$ at the TS is given by

$$P(j,E_V) \propto \Delta\phi(j,E_V) \qquad \text{(III.A.2)}$$

where $\Delta\phi(j,E_V)$ is the available ϕ angle range consistent with the constraint (see eq A.8.a)

$$V_B(\phi) \leq E_P - E_V - \frac{j^2}{2I} \qquad \text{(III.A.3)}$$

Figure 2 depicts the calculation of $P(j,E_v)$. In the left upper panel a, the right-hand part of eq III.A.3 is represented as a function of j. In the right upper panel b, $V_B(\phi)$ is represented in terms of ϕ. For a given value of j, the available ϕ angle range defined by eq III.A.3 is reported in the lower panel c according to the graphic procedure suggested by the dashed lines. The point P in pannel b corresponding to the hilltop at 90° is connected to the point P' in panel c. For j lower than j_P, the ϕ angle domain decreases smoothly since the potential walls are roughly parallel. For j larger than j_P, i.e., when the right-hand part of eq III.A.3 is lower than the energy of P, the ϕ angle domain is significantly shrunk leading to a more abrupt decrease of $P(j,E_v)$. Moreover, the larger E, the later the position

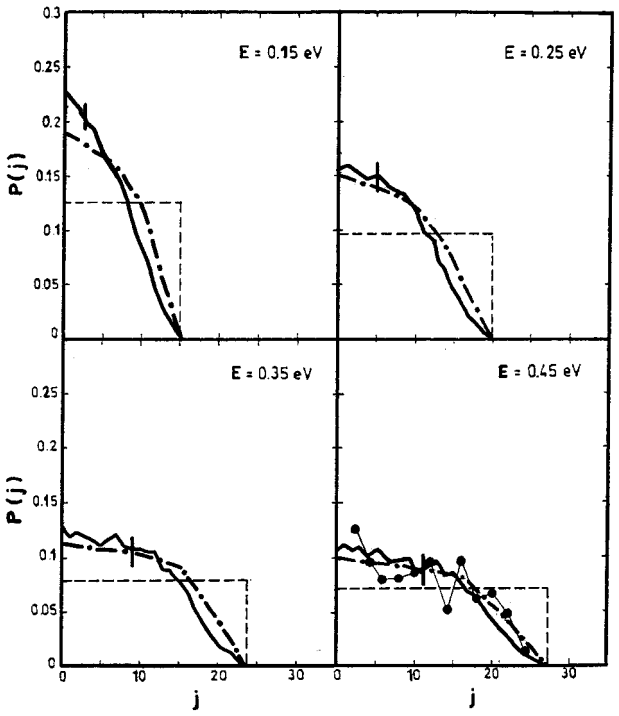

Figure 3. Rotational energy distribution $P(j,E_0)$ in the products of the reaction $O_2H \rightarrow O_2 + H$ for four values of the excess energy E; QCT (solid lines); PST according to our formulation (dashed lines); SACM highest populated states (vertical bars); our method (dashed−dotted lines); quantum results (filled circles joined by a thin solid line).

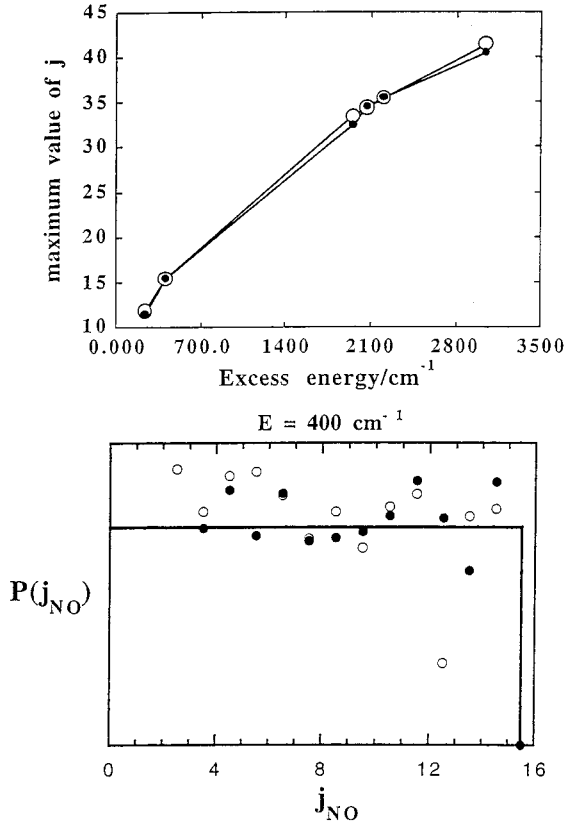

Figure 4. Upper panel: maximum value of j in terms of the excess energy E in the products of the reaction $NO_2 \rightarrow NO + O$; see the right eq C.3.b with $E_V = E_0$. Lower panel: rotational energy distribution $P(j,E_0)$. Experiment results shown by circles ($2\Pi_{1/2}$, filled circles; $2\Pi_{3/2}$, open circle), third expression of Table 2 by a solid line.

of the beak point P'. This can be observed in Figure 3 which is similar to Figure 15 extracted from ref 21. It represents $P(j,E_0)$ (for the lowest vibrational level of O_2) as obtained by Dobbyn et al.[21] for four resonance energies E (0.1513 eV, 0.2517, 0.3507, and 0.4471 eV) from four methods: QCT (thick solid curves), PST according to our formulation (short dashes), SACM highest populated states (vertical bars), and time-independent quantum approach (filled circles, thin solid line) in the fourth case. The quantum results are not those displayed in Figure 15 of ref 21 but an average of the rotational state distributions over five energies distributed in a small domain around 0.4471 eV (see Figure 9 in ref 21). Concerning the PST results, we have found that the maximum j values for each resonance energy E, that is,

$$j_{max}(E) = (2IE)^{1/2} \qquad \text{(III.A.4)}$$

are in much better agreement with dynamical results than those obtained with PST as implemented by Dobbyn et al. Equation III.A.4 has been deduced from eq A.8.a with $E_V = E_0$, $E_P - E_0 = E$ and $V(R^{\ddagger},r_e,\phi) = V_B(\phi) = 0$ ($\phi = 55°$ or $\phi = 125°$). The reduced moment of inertia I of the system is given by eq A.7, and the parameters used are given in the second row of Table 3. We have added our $P(j,E_0)$ results (dashed−dotted lines) obtained as described in Figure 2 (see also eq III.A.2 and III.A.3), $V_B(\phi)$ being approximated by the following polynomial expression

$$V_B(\phi) = \sum_{m=0}^{6} c_m \phi^m \qquad \text{(III.A.5)}$$

with $c_0 = -0.31625$, $c_1 = -0.1651$, $c_2 = -8.9653 \times 10^{-3}$, $c_3 = 1.9284 \times 10^{-4}$, $c_4 = -1.972 \times 10^{-6}$, $c_5 = 9.5758 \times 10^{-9}$, $c_6 = -1.7733 \times 10^{-11}$. The validity of our method is clearly demonstrated from the good agreement between our results and those from QCT. Dobbyn et al. showed that the rotational state distribution at the TS as obtained from the trajectories ($P^{\ddagger}_{QCT}$) agrees quite well with the rotational distribution obtained from a microcanonical selection at the TS ($P^{\ddagger}_{\mu}$), i.e., a random selection of the phase space states in the dividing surface (see Figure 17 in ref 21). Both are in very good agreement with eq III.A.2, which is not a surprise (at least for $P^{\ddagger}_{\mu}$) since eq III.A.2 is a consequence of the microcanonical assumption at the TS.

In the case of the reaction I.1 ($C_2H \rightarrow C_2 + H$), the total energy E_P ($\approx$0.5 eV) is roughly three times greater that the barrier height V_0. The recoil velocity between H and C_2 is sufficiently large in average for the bending forces not to have time enough to act (no funnel effect as shown in ref 18), preventing any rotational−translational energy transfer. Thus, there is no difference between product distributions at the TS and in the products. For reaction I.2 ($O_2H \rightarrow O_2 + H$), the total energy E_P ranging from 0.15 to 0.45 eV is hardly greater than the top of the hill ($\approx$0.27 eV) except in the fourth case (0.45 eV). Then, the recoil velocity of H with respect to O_2 is lower in average than that in the previous case and the system is more sensitive to the action of the bending forces. The funnel effect,[18] i.e., the decrease of the rotational angular momentum in favor of the recoil motion between the TS and the products, has more time to take place, especially for the smallest values of energy disposal. In other words, the lower the total energy, the larger the discrepancies between our statistical model and the dynamical approaches. Nevertheless, the agreement remains very satisfying in any case. As observed by Dobbyn et al., who analyzed in some detail the exit-channel effects occurring in reaction I.2, there is also a vibrational de-excitation (Figure 16

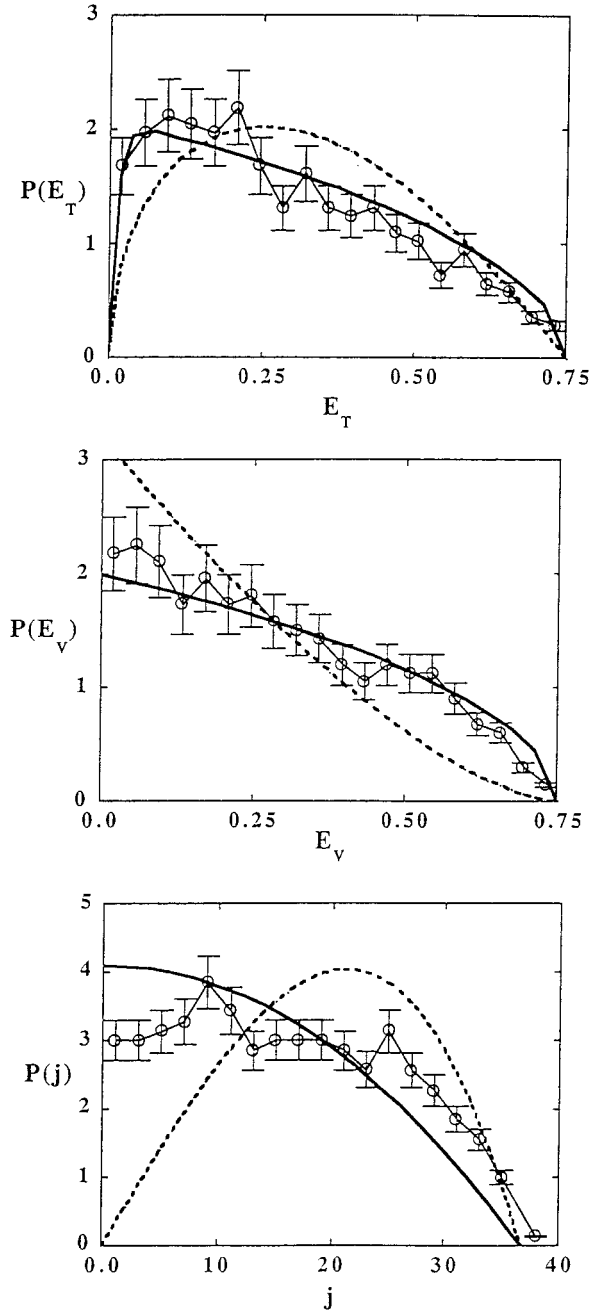

Figure 5. Product distributions for the reaction $Al_3 \rightarrow Al_2 + Al$; all the vibrational levels are taken into account in the rotational angular momentum distribution (fourth row in Table 2): QCT (open circles joined by thin solid lines), PST according to our formulation (thick solid lines), PDF (dashed lines).

in ref 21). It appears to be sufficiently small, however, for eq III.A.1 to be reasonable.

It is important to note, even for a hydrogen emission process for which quantum mechanical effects could be expected, the good accord between the average quantum results and the classical ones as mentioned by the authors of ref 21 (see Figure 3). This finding supports the idea that simple classical models may be very efficient in rationalizing energy partitioning in dynamical processes despite the quantum nature of nuclear motions. It should also be mentioned that our method is a classical analytical counterpart of the "mapping of transition-state wavefunctions" proposed by Reisler and co-workers,[24,21] and the similarity of the results obtained by both methods can be easily checked. Why it is so is an interesting question but the answer does not seem to be obvious.

B. Processes Governed by Long-Range Forces. Here, our method is applied to the reactions $NO_2 \rightarrow NO + O$[24] (eq I.3) and $Al_3 \rightarrow Al_2 + Al$[25] (eq I.4) which are governed by long-range forces, at least at low energies of a few kcal/mol. The values of the parameters used are given in Table 3. The results are given in Figure 4 (I.3) and Figure 5 (I.4) where PDF are also shown.[23] The agreement between the maximum j or the distributions obtained using our method and the experimental ones is again very satisfactory, which is not the case for the PDF.

IV. Conclusion

The findings of the present work follow.

(1) The energy distribution functions for barrier-type unimolecular reactions of the type $ABC \rightarrow AB + C$ where C is much lighter than A and B (typically a hydrogen atom) have been determined (see Table 1). For such processes, we have shown recently[18] that exit-channel coupling effects are negligible so that the energy partitioning is the same at the transition state—where the microcanonical postulate can be applied—and in the products.

(2) The energy distribution functions for three-atom unimolecular reactions governed by long-range forces (see Table 2) have been determined. Both sets of functions in Tables 1 and 2 are much more realistic than the prior distribution functions of Levine and Bernstein without being more complicated.

(3) The validity of these distributions in the following processes: (i) $C_2H \rightarrow C_2 + H$ (model alkyl dissociation reaction), (ii) $O_2H \rightarrow O_2 + H$, (iii) $NO_2 \rightarrow NO + O$, and (iv) $Al_3 \rightarrow Al_2 + Al$ has been verified.

(4) For (i) a barrier-type reaction and (ii) a reaction which is barrierless but involves strong angular anisotropies in the exit-channel part of the potential energy surface, the distributions derived from our method are much more realistic than those obtained using PST or SACM.

Acknowledgment. We are very grateful to Dr W. Forst for helpful advice in writing this paper.

Appendix A: General Procedure for the Derivation of an Energy Distribution at the Transition State

We present here the general procedure for the calculation of both the numerator and the denominator of eq II.1.

1. Coordinate System. The coordinate system used is represented in Figure 6. **r** is the vector joining A and B, and **R** is the one joining G and C where G is the center of mass of AB. ϕ is the angle between **r** and **R**. **j** and **L** are the rotational and orbital angular momenta. (x, y, z) is an arbitrary frame such that z is along **j**. Since **J** equals zero, we have $j = j_z = L = -L_z$. β_{AB} is the angle between the x-axis and **r**. β_C is the angle between the x-axis and **R**. A phase space state is thus completely defined by a set of seven variables (R, P_R, r, p_r, j, β_C, β_{AB}), where P_R and p_r are the momenta conjugate to R and r.

2. Energy Partitioning at the Transition State. Along the reaction path, from the TS to the products, E_V is supposed to be weakly coupled to E_R and E_T whatever the nature of the TS (for instance, see ref 8a, section III, point i). In this regard, vibrational modes are often termed conserved modes.[11] This is due to the fact that in many cases, the potential energy $V(R,r,\phi)$ can be written as

$$V(R,r,\phi) \approx v(r) + V(R,r_e,\phi) \quad \text{for} \quad R \geq R^{\ddagger} \qquad \text{(A.1)}$$

where $v(r)$ is the free potential energy of AB, $V(R,r_e,\phi)$ is the interaction potential energy between the rigid rotor AB (kept

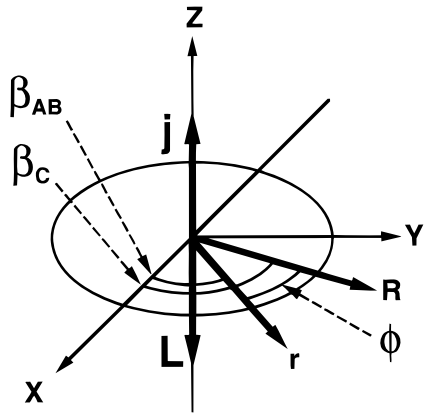

Figure 6. Coordinate system used in this work.

at its equilibrium distance r_e) and C, and $R^{\ddagger}$ gives the position of the TS. The classical Hamiltonian at the TS is

$$H = \frac{P_R^2}{2\mu} + \frac{L^2}{2\mu R^{\ddagger 2}} + \frac{p_r^{\,2}}{2m} + \frac{j^2}{2mr^2} + V(R^{\ddagger},r,\phi) \quad \text{(A.2)}$$

where m and μ are the reduced masses of AB and C with respect to AB. Accounting for eq A.1 and the rigid rotor (RR) approximation ($r = r_e$ in the AB-rotational term), H is given by the sum of the vibrational, rotational, and translational Hamiltonians H_V, H_R, and H_T defined as follows:

$$H_V = \frac{p_r^{\,2}}{2m} + v(r) \quad \text{(A.3)}$$

$$H_R = \frac{j^2}{2mr_e^{\,2}} \quad \text{(A.4)}$$

and

$$H_T = \frac{P_R^2}{2\mu} + \frac{L^2}{2\mu R^{\ddagger 2}} + V(R^{\ddagger},r_e,\phi) \quad \text{(A.5)}$$

3. Energy Constraints. Since $j = L(J{=}0)$, $H = E_P$, and $H_V = E_V$, we deduce from the previous expressions that

$$E_V + \frac{j^2}{2I} = E_P - V(R^{\ddagger},r_e,\phi) - \frac{P_R^2}{2\mu} \quad \text{(A.6)}$$

with

$$\frac{1}{I} = \frac{1}{mr_e^{\,2}} + \frac{1}{\mu R^{\ddagger 2}} \quad \text{(A.7)}$$

Since the relative kinetic energy $P_R^2/2\mu$ is larger than or equal to zero, eq A.6 leads to the following inequality which gives the range of variation of E_V and j for a given ϕ:

$$E_V + \frac{j^2}{2I} \le E_P - V(R^{\ddagger},r_e,\phi) \quad \text{(A.8.a)}$$

For analogous reasons, eq A.5 with $H_T = E_T$ implies:

$$E_T \ge V(R^{\ddagger},r_e,\phi) \quad \text{(A.8.b)}$$

Below, we also account for the fact that

$$E_V \ge E_0 \quad \text{(A.8.c)}$$

4. Flux Integrals. The fluxes $F(j,E_V,\phi,E)$ and $F(E_T,\phi,E)$ of trajectories crossing the TS with j, E_V, ϕ, and E on one hand and E_T, ϕ, and E on the other hand are formally given by

$$F(j,E_V,\phi,E) = \int d\Gamma \frac{P_R}{\mu} \prod_{i=1}^{5} \delta_i \quad \text{(A.9)}$$

and

$$F(E_T,\phi,E) = \int d\Gamma \frac{P_R}{\mu} \prod_{i=3}^{6} \delta_i \quad \text{(A.10)}$$

where $d\Gamma$ is the volume element defined by

$$d\Gamma = dR\, dP_R\, dr\, dp_r\, dj'\, d\beta_C\, d\beta_{AB} \quad \text{(A.11)}$$

and the δ_i's are as follows

$$\delta_1 = \delta(j' - j) \qquad \delta_2 = \delta(E_V - H_V)$$

$$\delta_3 = \delta(R - R^{\ddagger}) \qquad \delta_4 = \delta\left(\phi - \arccos\left(\frac{\mathbf{r}\cdot\mathbf{R}}{rR}\right)\right) \quad \text{(A.12)}$$

$$\delta_5 = \delta(E_P - H) \qquad \delta_6 = \delta(E_T - H_T)$$

Using a harmonic function for $v(r)$, eqs A.3 and A.5, the fact that

$$\arccos\left(\frac{\mathbf{r}\cdot\mathbf{R}}{rR}\right) = \beta_C - \beta_{AB} \quad \text{(A.13)}$$

(see Figure 6), and the theorem concerning the Dirac distribution of a function $f(x)$

$$\delta(f(x)) = \sum_{i=1}^{n} \frac{1}{|f'(x_i)|} \delta(x - x_i) \quad \text{(A.14)}$$

(with $f(x_i) = 0$ and $f'(x_i) \neq 0$, n being the number of simple roots), we find after some algebraic steps that

$$F(j,E_V,\phi,E) = 1 \quad \text{(A.15)}$$

and

$$F(E_T,\phi,E) = j_{max}(E_T,\phi,E) \quad \text{(A.16)}$$

where $j_{max}(E_T,\phi, E)$ is the maximum j consistent with E_T, ϕ, E and $J = 0$. (see Appendices B and C).

The fluxes $F(j,E_V,E)$, $F(E_V,E)$, $F(j,E)$, $F(E_R,E)$, $F(E_T,E)$, and $F(E)$ required for the derivation of energy distribution functions (see eq II.1) are deduced from $F(j,E_V,\phi,E)$ and $F(E_T,\phi,E)$ as follows:

$$F(j,E_V,E) = \int_{\phi_{min}(j,E_V,E)}^{\phi_{max}(j,E_V,E)} d\phi\, F(j,E_V,\phi,E)$$
$$= \phi_{max}(j,E_V,E) - \phi_{min}(j,E_V,E) \quad \text{(A.17)}$$

$$F(j,E) = \int_{E_{Vmin}(j,E)}^{E_{Vmax}(j,E)} dE_V\, F(j,E_V,E) \quad \text{(A.18)}$$

$$F(E_R,E) = \int dj\, F(j,E)\, \delta(E_R - j^2/2mr_e^2) \quad \text{(A.19)}$$

$$F(E_V,E) = \int_{j_{min}(E_V,E)}^{j_{max}(E_V,E)} dj\, F(j,E_V,E) \quad \text{(A.20)}$$

$$F(E_T,E) = \int_{\phi_{min}(E_T,E)}^{\phi_{max}(E_T,E)} d\phi\, F(E_T,\phi,E) \quad \text{(A.21)}$$

and

$$F(E) = \int_0^{j_{max}(E)} dj\, F(j,E) \quad \text{(A.22.a)}$$

$$F(E) = \int_{E_0}^{E_{Vmax}(E)} dE_V\, F(E_V,E) \quad \text{(A.22.b)}$$

$$F(E) = \int_{E_{Tmin}(E)}^{E} dE_T\, F(E_T,E) \quad \text{(A.22.c)}$$

All the boundaries involved in the above integrals are shown

to be deduced from eq A.8 in the following appendices. For the sake of convenience, we have ommited any constant involved in the developments leading to $F(j,E_V,\phi,E)$ and $F(E_T,\phi,E)$. This is unimportant since both the numerator and the denominator of relation II.1 are obtained by integrating either $F(j,E_V,\phi,E)$ or $F(E_T,\phi,E)$. In other words, the factor missing in the numerator of formula II.1 is also missing in the denominator.

Appendix B: Reactions Involving a Barrier

1. Rovibrational Energy Distributions. In this work, $V(R^{\ddagger},r_e,\phi)$ is assumed to be a quadratic function of ϕ, given by

$$V(R^{\ddagger},r_e,\phi) = V_0 + \frac{k}{2}(\phi - \phi_s)^2 \qquad \text{(B.1)}$$

ϕ_s defines the saddle point for which $V(R^{\ddagger},r_e,\phi)$ equals the barrier height V_0. Because of the symmetry of $V(R^{\ddagger},r_e,\phi)$ with respect to $\phi = \pi$, we limit ϕ to the range $[0, \pi]$. The actual fluxes are twice those derived in this condition but as explained at the end of Appendix A, this does not change the final result given by formula II.1. As shown previously, eqs A.8 and B.1 lead to the following boundary

$$E_{Vmin}(j,E) = E_0 \quad E_{Vmax}(j,E) = E_P - V_0 - \frac{j^2}{2I} \qquad \text{(B.2.a)}$$

$$j_{min}(E_V,E) = 0 \quad j_{max}(E_V,E) = (2I(E_P - V_0 - E_V))^{1/2} \qquad \text{(B.2.b)}$$

$$j_{max}(E) = (2I(E - V_0))^{1/2} \quad E_{Vmax}(E) = E_P - V_0$$
$$E_{Tmin}(E) = V_0 \qquad \text{(B.2.c)}$$

and because ϕ is limited to $[0, \pi]$, we have if $\phi_s = 0$ (linear TS)

$$\phi_{min}(j,E_V,E) = 0$$

$$\phi_{max}(j,E_V,E) = \left(\frac{2}{k}\left(E_P - V_0 - E_V - \frac{j^2}{2I}\right)\right)^{1/2} \qquad \text{(B.3.a)}$$

and if $\phi_s \neq 0$ (bent TS)

$$\phi_{min}(j,E_V,E) = \phi_s - \left(\frac{2}{k}\left(E_P - V_0 - E_V - \frac{j^2}{2I}\right)\right)^{1/2}$$

$$\phi_{max}(j,E_V,E) = \phi_s + \left(\frac{2}{k}\left(E_P - V_0 - E_V - \frac{j^2}{2I}\right)\right)^{1/2} \qquad \text{(B.3.b)}$$

Figure 7 shows cuts of the potential energy surface (PES) along the ϕ coordinate at the TS for both cases, $\phi_s = 0$ (linear TS) and $\phi_s \neq 0$ (bent TS). The ϕ boundaries are displayed in this figure.

Accounting for these limits and using the first four series of equations of Table 4, we arrive finally at the normalized $P(j,E_V)$, $P(j)$, $P(E_R)$, and $P(E_V)$ presented in Table 1. Treating the vibrational motion quantum mechanically leads to the following vibrational energy distribution:

$$P_V = \frac{(E_P - V_0 - \hbar\omega(v + {}^1/_2))}{\sum_{V=0}^{V_{max}}(E_P - V_0 - \hbar\omega(v + {}^1/_2))} \qquad \text{(B.4)}$$

2. Translational Energy Distribution. Let us now derive the recoil energy distribution $P(E_T)$. For a given E_T, the maximum E_R is equal to $E - E_T$. From relation A.4, the maximum value of j consistent with E_T and E is thus

$$j_M(E_T,E) = [2mr_e^2(E - E_T)]^{1/2} \qquad \text{(B.5.a)}$$

At the TS, the maximum value of L consistent with E_T and ϕ, deduced from eqs A.5 (where H_T has been replaced by E_T and P_R has been kept at zero) and B.1 is

$$L_M(E_T,\phi) = R^{\ddagger}\left[2\mu\left(E_T - V_0 - \frac{k}{2}(\phi - \phi_s)^2\right)\right]^{1/2} \qquad \text{(B.5.b)}$$

Since $j = L$, j cannot exceed $L_M(E_T,\phi)$. Therefore, the maximum value $j_{max}(E_T,\phi,E)$ of j consistent with E_T, ϕ, and E and the constraint $J = 0$ is given by

$$j_{max}(E_T,\phi,E) = \min[L_M(E_T,\phi); j_M(E_T,E)] \qquad \text{(B.6)}$$

By also using eqs A.5 (where H_T has been replaced by E_T and both P_R and L have been kept at zero) and B.1, we arrive at

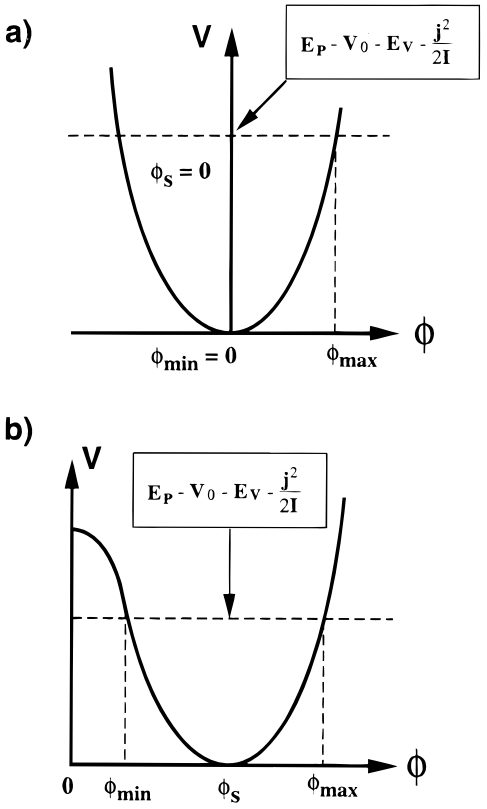

Figure 7. Cuts of the harmonic potential energy surface (PES) along the ϕ coordinate at the location of the transition state (TS) and minimum and maximum values of the ϕ angle: (a) in the case $\phi_s = 0$ (linear TS); (b) in the case $\phi_s \neq 0$ (nonlinear TS). In case b, there is another TS corresponding to $-\phi_s$. These two TS's are connected via a maximum at $\phi = 0$. This maximum is supposed to be sufficiently high to justify the harmonic approximation of the PES around ϕ_s. Moreover, the bending force constant k (see formula B.1) is supposed to be large enough for ϕ_{max} to be lower than π. It justifies the validity of formula B.3.

TABLE 4: Numbering of the Equations Necessary for the Calculation of Energy Distributions in the Products of Three-Atom Unimolecular Reactions Involving a Barrier

$P(j,E_V)$	eqs B.3, A.17, B.2.a, A.18, B.2.c, A.22.a, II.1
$P(j)$	same eqs as above
$P(E_R)$	same eqs as above + eq A.19
$P(E_V)$	eqs B.3, A.17, B.2.b, A.20, B.2.c, A.22.b, II.1
$P(E_T)$	eqs B.5, B.6, A.16, B.7, A.21, B.2.c, A.22.c, II.1

$$\phi_{min}(E_T,E) = \max\left[0; \phi_s - \left(\frac{2}{k}(E_T - V_0)\right)^{1/2}\right]$$

$$\phi_{max}(E_T,E) = \phi_s + \left(\frac{2}{k}(E_T - V_0)\right)^{1/2} \qquad \text{(B.7)}$$

$P(E_T)$ (last expression in Table 1) is found using the set of formulas indicated in the last row of Table 4.

Appendix C: Reactions Governed by Long-Range Forces

1. Rovibrational Energy Distributions. As explained in section II.C, the system is expected to behave as if the TS were defined by $R^{\ddagger} \approx b_{av}$ where $V(R^{\ddagger},r_e,\phi) \approx 0$, so that formulas A.8.a and A.8.c result in

$$E_0 \le E_V \le E_P - \frac{j^2}{2I} \qquad \text{(C.1)}$$

with

$$\frac{1}{I} = \frac{1}{mr_e^{\,2}} + \frac{1}{\mu b_{av}^{\,2}} \qquad \text{(C.2)}$$

On the other hand, formula A.8.b does not impose any constraints other than $E_T \ge 0$, which is true by definition. The boundaries in integrals A.18, A.20, and A.22 are therefore

$$E_{Vmin}(j,E) = E_0 \qquad E_{Vmax}(j,E) = E_P - \frac{j^2}{2I} \qquad \text{(C.3.a)}$$

$$j_{min}(E_V,E) = 0 \qquad j_{max}(E_V,E) = (2I(E_P - E_V))^{1/2} \qquad \text{(C.3.b)}$$

$$j_{max}(E) = (2IE)^{1/2} \qquad E_{Vmax}(E) = E_P \qquad E_{Tmin}(E) = 0 \qquad \text{(C.3.c)}$$

whereas those in integral A.17 are (ϕ does not appear in constraints C.1)

$$\phi_{min}(j,E_V,E) = 0 \qquad \phi_{max}(j,E_V,E) = 2\pi \qquad \text{(C.4)}$$

The normalized $P(j,E_V)$, $P(j)$, $P(E_R)$, and $P(E_V)$ presented in Table 2 are determined by using the series of equations given in the four first row of Table 5. If the vibrational motion is treated quantum mechanically, the other degrees of freedom still being treated by classical mechanics, $P(E_V)$ becomes

$$P_V = \frac{(E_P - \hbar\omega(v + {}^1/_2))^{1/2}}{\sum_{V=0}^{V_{max}} (E_P - \hbar\omega(v + {}^1/_2))^{1/2}} \qquad \text{(C.5)}$$

where $\hbar\omega$ is the vibrational energy quantum of AB.

2. Translational Energy Distribution. For a given E_T, the maximum E_R is equal to $E - E_T$. From relation A.4, the maximum value of j consistent with E_T and E is thus

$$j_M(E_T,E) = [2mr_e^{\,2}(E - E_T)]^{1/2} \qquad \text{(C.6)}$$

However, the relation $j = L$ implies that j cannot exceed $L_M(E_T)$ given by eq II.2′. Therefore, $j_{max}(E_T,\phi,E)$ is given by

$$j_{max}(E_T,\phi,E) = \min[L_M(E_T); j_M(E_T,E)] \qquad \text{(C.7)}$$

Obviously, this quantity does not depend on ϕ due to the spherical symmetry of the potential energy. For the same reason, we have

$$\phi_{min}(E_T,E) = 0 \qquad \phi_{max}(E_T,E) = 2\pi \qquad \text{(C.8)}$$

$P(E_T)$ (last row of Table 2) is found using the series of equations given in the last row of Table 5.

TABLE 5: Numbering of the Equations Necessary for the Calculation of Energy Distributions in the Products of Three-Atom Unimolecular Reactions Governed by Isotropic Long-Range Forces

$P(j,E_V)$	eqs C.4, A.17, C.3.a, A.18, C.3.c, A.22.a, II.1
$P(j)$	same eqs as above
$P(E_R)$	same eqs as above + eq A.19
$P(E_V)$	eqs C.4, A.17, C.3.b, A.20, C.3.c, A.22.b, II.1
$P(E_T)$	eqs II.2′, C.6, C.7, C.8, A.21, C.3.c, A.22.c, II.1

References and Notes

(1) Levine, R. D.; Bernstein, R. B. *Molecular Reaction Dynamics and Chemical Reactivity*; Oxford University Press: Oxford, 1987.

(2) See for example: Herschbach, D. R. *The Chemical Bond*; Zewail, A., Ed.; Academic Press: San Diego, CA, 1992; Chapter 8 and references therein.

(3) Polanyi, J. C. *Science* **1987**, *236*, 680.

(4) Halvick, P.; Rayez, J. C. *Chem. Phys.* **1987**, *114*, 375.

(5) Light, J. C. *J. Chem. Phys.* **1964**, *40*, 3221. Pechukas, P.; Light, J. C. *J. Chem. Phys.* **1965**, *42*, 3281. Light, J. C.; Lin, J. *J. Chem. Phys.* **1965**, *43*, 3209. Pechukas, P.; Light, J. C.; Rankin, C. *J. Chem. Phys.* **1966**, *44*, 794.

(6) Nikitin, E. E. *Theory of elementary atomic and molecular proceses in gases*; Clarendon Press: Oxford, 1974; Sections 28−31 and 50 and references therein.

(7) Safron, S. A.; Weinstein, N. D.; Herschbach, D. R.; Tully, J. C. *Chem. Phys. Lett.* **1972**, *12*, 564.

(8) (a) Quack, M.; Troe, J. *Ber. Bunsen-Ges. Phys. Chem.* **1974**, *78*, 240. (b) *Ibid.* **1975**, *79*, 170. (c) *Ibid.* **1976**, *80*, 1140.

(9) Klots, C. E. *J. Chem. Phys.* **1976**, *64*, 4269.

(10) Chesnavich, W. J.; Bowers, M. T. *J. Am. Chem. Soc.* **1976**, *98*, 8301.

(11) Wardlaw, D. M.; Marcus, R. A. *Adv. Chem. Phys.* **1988**, *70*, 231.

(12) Nadler, I.; Noble, M.; Reisler, H.; Wittig, C. *J. Chem. Phys.* **1985**, *82*, 2608. Qian, C. X. W.; Noble, M.; Nadler, I.; Reisler, H.; Wittig, C. *J. Chem. Phys.* **1985**, *83*, 5573. Wittig, C.; Nadler, I.; Reisler, H.; Catanzarite, J.; Radhakrishnan, G. *J. Chem. Phys.* **1985**, *83*, 5581.

(13) Bonnet, L.; Rayez, J. C. *Chem. Phys.* **1995**, *201*, 203.

(14) Miller, W. B.; Safron, S. A.; Herschbach, D. R. *Discuss. Faraday Soc.* **1967**, *44*, 108. Herschbach, D. R. *Discuss. Faraday Soc.* **1973**, *55*, 233. Safron, S. A. Ph.D. Thesis, Harvard University, 1969.

(15) Bonnet, L.; Rayez, J. C. *J. Chem. Phys.* **1995**, *102*, 9512.

(16) Hase, W. L. In *Potential Energy Surfaces and Dynamics Calculations*; Truhlar, D., Ed.; Plenum Press: New York, 1981; pp 23−24.

(17) Baer, T.; Hase, W. L. *Unimolecular Reaction Dynamics*; Oxford University Press: Oxford, 1996.

(18) Bonnet, L.; Rayez, J. C. *J. Chem. Phys.* **1995**, *103*, 2929.

(19) Bush, G.; Wilson, K. *J. Chem. Phys.* **1972**, *56*, 3626. Tuck, A. *J. Chem. Soc., Faraday Trans. 2* **1977**, *73*, 689. Levene, H.; Valentini, J. *J. Chem. Phys.* **1987**, *87*, 2594. Chen, I. C.; Moore, C. B. *J. Phys. Chem.* **1990**, *94*, 269.

(20) (a) Wolf, R. J.; Hase, W. L. *J. Chem. Phys.* **1980**, *72*, 316; **1981**, *75*, 3809; (b) **1980**, *73*, 3010. Hase, W. L.; Bhalla, K. C. *J. Chem. Phys.* **1981**, *75*, 2807. (c) Hamilton, I.; Brumer, P. *J. Chem. Phys.* **1985**, *82*, 595.

(21) Dobbyn, A. J.; Stumpf, M.; Keller, H. M.; Schinke, R. *J. Chem. Phys.* **1996**, *104*, 8357.

(22) Schinke, R. *Photodissociation dynamics, Cambridge Monographs on Atomic, Molecular and Chemical Physics*; Cambridge University Press: Cambridge, 1993; p 9.

(23) See ref 1, page 275.

(24) Reid, S. A.; Reisler, H. *J. Phys. Chem.* **1996**, *100*, 474 and references therein.

(25) Peslherbe, G. H.; Hase, W. L. *J. Chem. Phys.* **1994**, *101*, 8535.

(26) Brucker, G. A.; Ionov, S. I.; Chen, Y.; Wittig, C. *Chem. Phys. Lett.* **1992**, *194*, 413.

(27) Pastrana, M. R.; Quintales, L. A. M.; Brandao, J.; Varandas, A. J. *J. Phys. Chem.* **1990**, *94*, 8073.